NANO LETTERS

Letter

pubs.acs.org/NanoLett

Tunable Metallic Conductance in Ferroelectric Nanodomains

Peter Maksymovych,*[,†] Anna N. Morozovska,[‡,§] Pu Yu,[∥] Eugene A. Eliseev,[§] Ying-Hao Chu,[∥,⊥] Ramamoorthy Ramesh,[∥] Arthur P. Baddorf,[†] and Sergei V. Kalinin[†]

[†]Center for Nanophase Materials Sciences, Oak Ridge National Laboratory, Oak Ridge, Tennessee 37831, United States

[‡]Institute of Semiconductor Physics, National Academy of Science of Ukraine, 41, pr. Nauki, 03028 Kiev, Ukraine

[§]Institute for Problems of Materials Science, National Academy of Science of Ukraine, 3, Krjijanovskogo, 03142 Kiev, Ukraine

[∥]Department of Materials Science and Engineering and Department of Physics, University of California, Berkeley, California 94720, United States

[⊥]Department of Materials Science and Engineering, National Chiao Tung University, Hsinchu, Taiwan 30010

Supporting Information

ABSTRACT: Metallic conductance in charged ferroelectric domain walls was predicted more than 40 years ago as the first example of an electronically active homointerface in a nonconductive material. Despite decades of research on oxide interfaces and ferroic systems, the metal−insulator transition induced solely by polarization charges without any additional chemical modification has consistently eluded the experimental realm. Here we show that a localized insulator−metal transition can be repeatedly induced within an insulating ferroelectric lead-zirconate titanate, merely by switching its polarization at the nanoscale. This surprising effect is traced to tilted boundaries of ferroelectric nanodomains, that act as localized homointerfaces within the perovskite lattice, with inherently tunable carrier density. Metallic conductance is unique to nanodomains, while the conductivity of extended domain walls and domain surfaces is thermally activated. Foreseeing future applications, we demonstrate that a continuum of nonvolatile metallic states across decades of conductance can be encoded in the size of ferroelectric nanodomains using electric field.

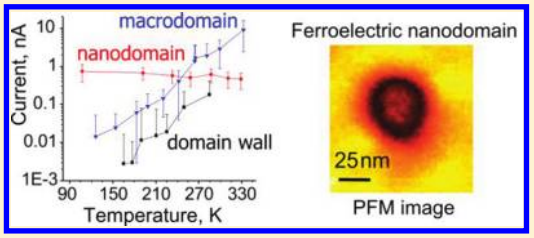

KEYWORDS: *Ferroelectric, domain wall, MIT, metallic, lead-zirconate, scanning probe microscopy*

Oxide interfaces have developed into a new nanoscale medium for emergent electronic properties.[1] Recent examples include two-dimensional electron gas[2] and magnetism[3] formed at an epitaxial boundary between band insulators, tunable electronic correlations at an interface between a Mott and band insulators,[4] surface conductivity[5,6] and superconductivity[7] of an insulator, and coupling of order parameters across the interface.[8,9] Though rich in behaviors, oxide heterointerfaces are defined by an abrupt change of chemical composition, significantly restricting the ability to move and pattern the interface or modify its structure. Such modifications not only lead to new applications but are also critical for the fundamental understanding of emergent properties.

On the other hand, a distinct oxide interface can be defined by the change of lattice symmetry, rather than its chemical composition,[10] in which case it can be continuously patterned with applied fields. Such homointerfaces are ubiqitous in ferroelectric and multiferroic materials, occurring as topological defects of the ferroelectric order parameter in the form of domain walls,[11] junctions,[12] and vortices.[13,14] The emergence of unique electronic and magnetic properties of ferroic homointerfaces can thus make them a viable alternative to chemically defined heterointerfaces.[10]

The archetypal proposal for an electronically active ferroic homointerface is a charged domain wall in a ferroelectric crystal. Accumulation of compensating carriers that screen the bound charge of such a domain wall should in principle enable a localized insulator−metal transition. Although this basic proposal has been put forth theoretically a number of times since the early 1970s,[15−17] the experimental demonstration of ferroelectrically controlled metal−insulator transition has been lacking. Several recent experiments, most notably in $BiFeO_3$[18] and more recently $PbZr_{0.2}Ti_{0.8}O_3$,[19] revealed that ferroelectric domain walls can be conducting. However, electron transport has so far been to thermally activated hopping mechanisms.[18−20] Furthermore, as it is notoriously difficult to separate the bulk and interfacial components of electronic conduction,[21,22] identifying the domain wall as a conduction pathway throughout the material (as opposed to modification of the interface) is ambiguous in the case of thermally activated mechanisms.

Here, we have utilized nanoscale ferroelectric switching to activate metallic conduction through an otherwise insulating lead-zirconate titanate, $PbZr_{0.2}Ti_{0.8}O_3$ (PZT) film. In contrast to previous works,[18,19,23,24] which avoided the regime of ferroelectric switching in the search for electronic properties, we have invoked scanning probe microscopy to monitor the

Received: September 26, 2011
Revised: December 9, 2011
Published: December 19, 2011

   dx.doi.org/10.1021/nl203349b | *Nano Lett.* 2012, 12, 209−213

conductivity of ferroelectric nanodomains, as they are locally created under the tip and subsequently evolve in the electric field. It is in these inherently nanoscale entities that we have found the long-sought metallic conductivity. Other entities on the surface, such as domain walls and domains themselves have only exhibited the expected thermally activated conduction. This dramatic contrast in the electronic properties unambiguously identifies a new and highly localized conduction channel through the insulating ferroelectric oxide, created by nanodomains. Our theoretical analysis concludes that the tilt angle of the domain wall, which naturally emerges in the nanodomain, is the key enabling step to metallic conductivity due to a combination of charge and flexoelectric effects. Furthermore, both experimental measurements and theoretical analysis revealed that the metallic conductivity is tunable by electric field, through the changes of size of the nandomain and, correspondingly, the tilt of its domain wall. This phenomenon is a new manifestation of the notorious ferroelectric field effect,[25] involving a homointerface rather than a heterointerface of a ferroelectric material. We expect that the observed effects will be universal to ferroelectric semiconductors, opening a new family of electronic properties that will break new grounds in fundamentals and applications alike.

Systematic studies of $I-V$ curves and spatially resolved conductance on the surfaces of 30 and 50 nm epitaxial PZT films using conductive atomic force microscopy in ultrahigh vacuum have revealed three kinds of electronic behavior, summarized in Figure 1: (1) strongly hysteretic $I-V$ curves associated with an upward-polarized nanoscale domain, henceforth referred to as a nanodomain (Figure 1A); (2) negligibly hysteretic $I-V$ curve on the surface of the upward-polarized domain with the linear dimension exceeding 100 nm, henceforth referred to as macrodomain (Figure 1A); and (3) finite conductivity of ferroelectric domain walls separating mesoscopic regions of downward and upward polarization (Figure 1C,D and Supporting Information Figure S1) with direct analogy to conductive domain walls in multiferroic $BiFeO_3$[18] and consistent with the recent measurements on the PZT film of similar composition.[19] In line with our previous study on a similar PZT material,[26] the hysteresis of the $I-V$ curves from the nanodomains is associated with the process of their creation, that is, with the localized polarization switching from the downward to upward orientation of spontaneous electrostatic polarization. This is further confirmed by simultaneously monitored surface displacement, where discontinuities in the characteristic "butterfly"-shaped loops (Figure 1B, top) identify polarization switching events and coincide within the measurement bandwidth with the discontinuity in the $I-V$ curve at the positive sample bias (~ 4 V in Figure 1B bottom).[26] A complete lack of any conductive features at the opposite (negative) switching voltage bias (Figure 1B), where the nanodomain disappears, rules out interpretation of resistive switching as due to displacement current or extrinsic capacitive effects accompanying polarization reversal. Notably, polarization-controlled conductance at the negative switching voltage with a comparable outcome to the positive switching voltage could also be observed, (Supporting Information Figure S3), after creating specific ferroelectric domain geometries as detailed in the Supporting Information.

As seen in Figure 1, the nanodomain is the most conducting entity on the PZT surface and its nucleation coincides with up to 4 orders of magnitude increase of local conductance (Figure 1A). Most surprisingly, however, is that although both domain

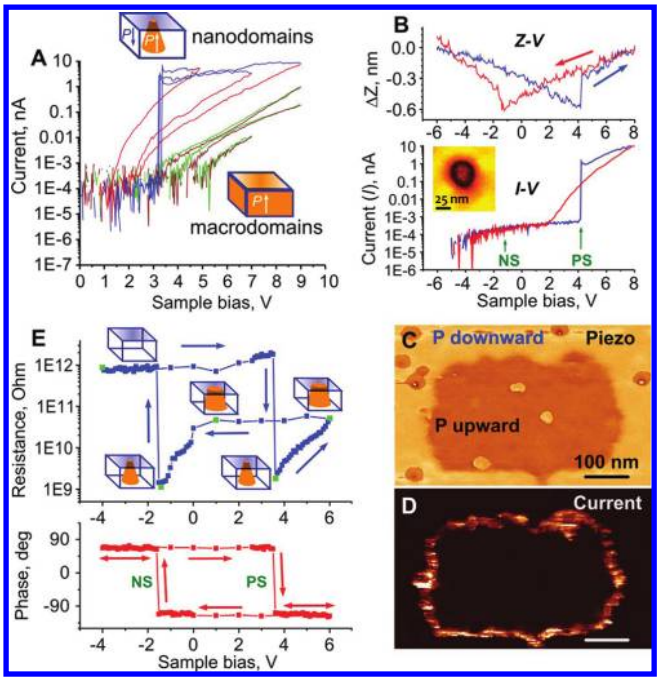

Figure 1. (A) Representative hysteretic $I-V$ curves from upward polarized ferroelectric nanodomains on the 50 nm $PbZr_{0.2}Ti_{0.8}O_3$ film (blue, forward; red, reverse), and nonhysteretic $I-V$ curves from macrodomains on the same surface (green, forward; brown, reverse). Only sample bias range >0 V is shown for clarity. (B) Top: hysteresis in surface displacement (top) associated with appearance of the nanodomain in the transport junction. Polarization switching is registered by discontinuities in the displacement loop. The arrows follow the direction of the forward (blue) and backward (red) voltage ramps. Bottom: hysteresis in current acquired simultaneously with the hysteresis in surface displacement. PS and NS mark the positive and negative switching voltages, as judged from the displacement loop. Insert shows a piezoresponse amplitude image of a representative nanodomain, imaged shortly after its formation under the tip. (C,D) Simultaneously acquired images of piezoresponse ($A\sin(\phi)$, where A is amplitude and ϕ is phase of piezoresponse), (C), and current, (D), at 2.5 V sample bias, revealing finite conductivity of domain walls in $PbZr_{0.2}Ti_{0.8}O_3$. (E) Top: local resistance of the PZT film at sample bias of 2.6 V acquired using a pulse-probe waveform (see Supporting Information for details). Cartoon schematics show nanodomains of upward polarization orientation (orange) believed to be formed at various instances of the resistance curve (green points). Bottom: phase of local piezoresponse accompanying the resistance curve. Phase flip by 180° registers polarization switching events. The arrows follow the direction of the voltage waveform.

walls and macrodomains are governed by thermally activated conduction (Figure 2A) with a barrier from 100 to 250 meV (extracted from an Arrhenius fit), the nanodomain conductance is negligibly temperature-dependent, irrespectively of the probing bias (at least up to 9 V), forward or reverse branch of the $I-V$ curve or even the measurement protocol used to acquire the $I-V$ curve (Figure 2). This unexpected departure from the anticipated hopping conduction mechanism for PZT[27,28] signals a fundamentally distinct electron transport regime in the nanodomains and new nanoscale electronic effects at the instance of polarization switching.

Of the likely candidates, only two transport mechanisms exhibit nonactivated temperature dependence, similar to our case: electron tunneling and metallic conductivity (by analogy with the temperature-dependent conductance of "bad metals" and doped $SrTiO_3$ in particular[29−31]). As discussed in the

dx.doi.org/10.1021/nl203349b | Nano Lett. 2012, 12, 209−213

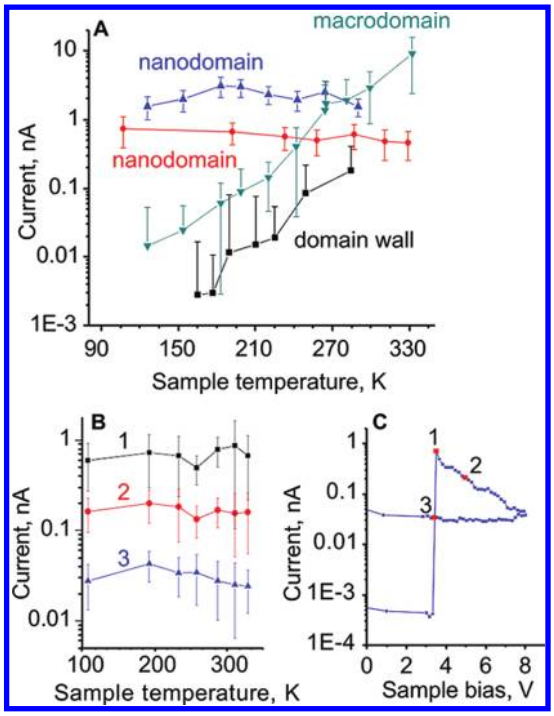

Figure 2. (A) Temperature-dependence of local current obtained from averages of ~100 hysteretic $I-V$ curves on nanodomains (blue, measured at 4.5 V), ~50 resistive curves on nanodomains (red, measured at 3.5 V), ~100 nonhysteretic $I-V$ curves on macrodomains (green, measured at 7 V) and one current image (similar to Figure 1D) from the domain walls (measured at 2.6 V) at each temperature. Error bars are standard deviation for each data set. (B) Temperature-dependence of the tunable conductivity of nanodomains as a function of their size: black, smallest (at creation); red, intermediate; and blue, average equilibrium size at sample bias of 8 V. Each point on the plot is an average of ~50 measurements. (C) A typical resistance curve at T = 329 K, showing the values (red), dependent on domain sizes, that were sampled in Figure 2B.

following, we believe that both mechanisms are operating in series in the nanodomains.

The $I-V$ curves from the nanodomains (Figure 1) clearly favor tunneling, closely resembling the Fowler–Nordheim tunneling mechanism across a thin, approximately triangular tunneling barrier.[26] However, given that the studied films are 30–50 nm thick, tunneling cannot occur across the whole film thickness, and the $I-V$ curves must in general be also influenced by the bulk region of the nanodomain.[21,22] In fact, two independent measurements imply that the bulk conductance is comparable to that of contact tunneling in our case. A similarly grown 30 nm PZT film (Supporting Information Figure S2) shows significantly higher conductance than the 50 nm film (because of the shorter effective bulk region and its resistance). At the same time, the conductance of the nanodomains is tunable. This is evidenced by monitoring local resistance of the PZT film along the ferroelectric switching cycle in Figure 1E, where the net resistance is smallest right after polarization switching (at ~4 V) and gradually increases with increasing sample bias, which in turn increases the size of the nanodomain (see Supporting Information for further discussion of Figure 1E). The size-dependence of nanodomain conductance is also manifested in Figure 1A, where a unique reverse (red) $I-V$ curve is produced for a given nanodomain by increasing the peak magnitude of applied positive bias. Crucially, the tunable conductance of nanodomains must involve both bulk and surface components of conductivity, implying that they are comparable in magnitude. Indeed, if we attributed tunable conductance solely to the properties of the tip–surface tunneling contact, nanodomains would exhibit similar temperature-dependence to that of macrodomains (as is the case of the domain wall in Figure 2A), because the tip–surface contact would be evidently more conducting in nanodomains (based on comparison of $I-V$ curves for nanodomain and macrodomains in Figure 1A) and thus less transport limiting. Finally, comparable magnitude of the interfacial and bulk conductance together with the temperature-independence of the net conductance in Figure 2A imply that both surface and bulk mechanisms exhibit negligible temperature-dependence. Thus the key signature of the ferroelectric nanodomains is that it creates a metallic conduction path that connects the surface and the bottom interface of the PZT film. The pathway may be located within the nanodomain and/or immediately adjacent to its domain walls.

Nanodomains represent a single nucleus of opposite polarization, and will in general be decorated by curved domain walls.[32,33] The shape anisotropy is determined by the competition between domain wall pinning strength, anisotropic depolarization field and domain wall motion in the strongly inhomogeneous electric field of the biased metal tip. Irrespective of the detailed hypothesis regarding the transport mechanism, curved and tilted domain boundaries of the nanodomain will produce bound polarization charges along the walls (as schematically shown in Figure 3A). We believe that the primary reason for the metallic conductivity is a local modification of the carrier density due to accumulation of compensating charge that screens this large bound polarization charge at a tilted domain wall. Accumulation of compensating charge on tilted and curved domain walls has, in fact, been considered theoretically in several papers, dating as far back as the early 1970s.[15−17,34]

We have modeled tilted 180° domain walls (by angle θ with respect to the surface normal) in an n-type ferroelectric-semiconductor PZT with intrinsic oxygen vacancies (donors) and free electrons, using coupled Landau–Ginzburg–Devonshire and Poisson equations (see Supporting Information for details). Domain wall tilt was found to increase the local density of free (compensating) carriers by up to 3 orders of magnitude (Figure 3A,B). If we assume that conductivity is directly proportional to carrier density, accumulation of compensating carriers will translate into up to 3 orders of magnitude increase of local conductivity ($\sigma(\xi)$) compared to the parent matrix. Furthermore, tilted domain walls can control not only the density but also the type of accumulated carriers with electron accumulation for upward polarized nanodomains in the downward polarized matrix, and hole accumulation for the opposite relative polarization orientations.

Additional accumulation results from flexoelectric coupling in PZT, existing even for a nominally uncharged cylindrical wall (see Supporting Information for details). Here, the polarization component perpendicular to the wall surface ($P_\perp$) occurs due to strain gradients with a maximal value of $P_\perp(\xi = \pm w) \approx \pm f_{12}\varepsilon_0\varepsilon_b[(Q_{11} + Q_{12})P_S^2]/[(s_{11} + s_{12})w]$ (f_{12} is the flexoelectric coupling coefficient, s_{ij} is the elastic compliances, P_S is the spontaneous polarization, $w = 2r_c\sqrt{2} \sim 1$ nm is the half-width of uncharged wall, Q_{ij} is the electrostriction coefficients, ε_0 and ε_b are the respective permittivities of vacuum and nonferro-

dx.doi.org/10.1021/nl203349b | Nano Lett. 2012, 12, 209–213

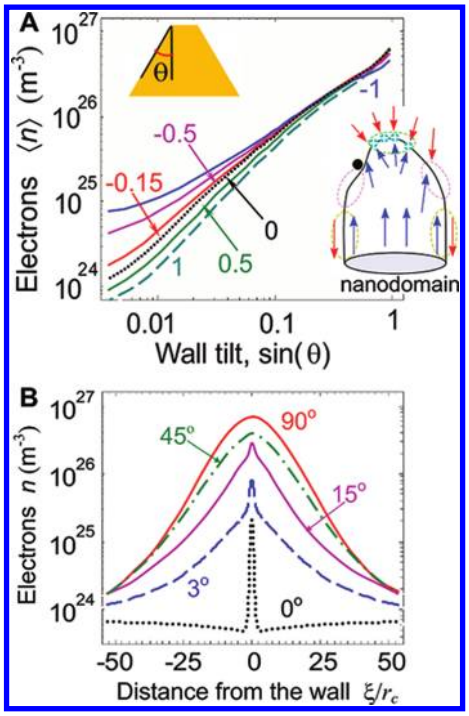

Figure 3. (A) Dependence of the carrier concentration $\langle n(\xi)\rangle$ averaged across the wall thickness on the wall tilt, sin θ. Calculations were performed for the head-to-head 180° walls and with different flexoelectric coupling coefficient f_{12} = (−1, −0.5, −0.15, 0, 0.5, 1) × 10^{-10} m^3/C (as labeled). Inserts show the definition of angle θ and a schematic of a nanodomain exhibiting both straight (uncharged, yellow outline) c+/c− and curved (slightly charged, purple outline; strongly charged, green outline) domain walls, the associated directions of spontaneous polarization (blue and red arrows) and a defect (black). (B) Dependence of electron density for 180° domain wall with different slope angles θ = 90, 45, 15, 3, and 0° as a function of distance (ξ/r_c) perpendicular to the domain wall (correlation length $r_c \approx 0.5$ nm).

electric background). Flexoelectric coupling produces local built-in depolarization field $\delta E_{max} \approx f_{12}[(Q_{11} + Q_{12})P_S^2]/[w(s_{11} + s_{12})]$, that in turn leads to the carrier accumulation along the wall with up to 10-fold increase of domain wall conductivity (Figure 3A).

Tunability of metallic conductance in nanodomains, implied by the theoretical model, was indeed observed experimentally by measuring the temperature-dependence of nanodomain conductance as a function of its size, at several points of the resistance change curve (Figure 1E, 2C). The whole range of nanodomain dimensions probed in our experiment, spanning approximately 1.5 orders of magnitude of conductance (Figure 2B), revealed negligible temperature dependence. At present we cannot strictly rule out alternative explanations of metallic conductivity, for example, formation of an impurity band at the domain wall through the local increase of the dielectric constant ε and/or accumulation of donor (acceptor) impurities (similar to the hypothesis for $SrTiO_3$ at low doping[31]), or an altogether different nontrivial interaction of the domain wall with extended defects.[29] However, the fact that domain walls of a macroscopic domain (with presumably equilibrated straight shape across the film thickness) exhibit temperature-dependent conduction (Figure 1C, 2A) attests to the notion that the domain wall curvature and the ensuing electrostatic effects are central to metallic conductivity.

Aside from the prospects in novel fundamental properties of ferroelectrics and related multiferroic materials that may originate from tunable and metallic conductivity in nanodomains, the present findings also significantly expand the original concept of switchable tunneling conductance across ultrathin ferroelectrics.[35] The latter was motivated by the need of nondestructive read-out of FeRAM nonvolatile memory elements and their efficient downsizing to the nanoscale regime. On one hand, metallic conductivity provides a controlled route to achieve large absolute currents in the 1−100 nA range (Figure 1A) in relatively thick films (up to 50 nm thick in our case). Thick films are both more readily applicable than ultra narrow tunnel junctions and can also be sculpted in the form of superlattices in search of new properties. On the other hand, the wide dynamic range of the nanodomain dimensions between a small nucleus and a macrodomain translates into the respectively tunable conductance property of a bistable ferroelectric (i.e., with polarization either up or down). Figure 4A demonstrates that multiple distinct

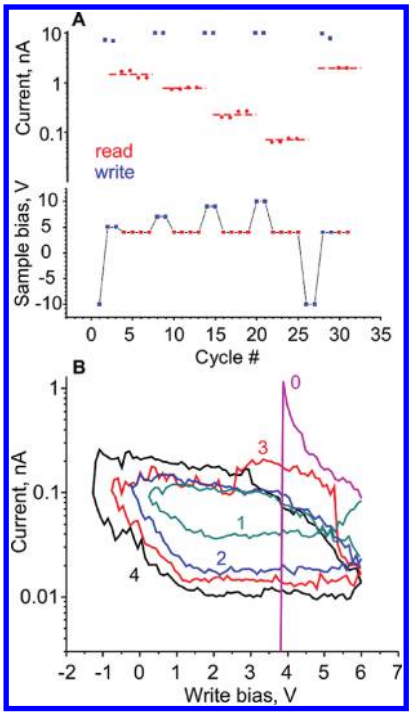

Figure 4. (A) Five nonvolatile resistive states of a single nanodomain (top) created by a series of voltage pulses shown at the bottom. Local current during both read (red) and write (blue) steps are shown. Dashed lines are a guide to the eye, approximately showing the average current for each of the resistive states. (B) Resistance curves showing nondestructive and repeated manipulation of the size and shape of the nanodomain, reflected in the corresponding change of local current. After the first step of creating the nanodomain (step 0, purple), subsequent cycling of the sample bias in a chosen limited range (steps 1−4) results in a continuous change of local current, testifying that the nanodomain does not disappear, but local current can nonetheless be repeatedly varied between high and low conductance states.

conductance states can be created at a single surface location by an appropriate selection of the set-pulse. Furthermore, once the appropriate nanodomain has been created (cycle 0 in Figure 4B), tunable conductance states can be repeatedly manipulated without erasing the nanodomain, merely by changing its size as shown by cycles 1−4 in Figure 4B.

dx.doi.org/10.1021/nl203349b | Nano Lett. 2012, 12, 209−213

In summary, from a comprehensive analysis of local electronic conductance of the ferroelectric surface of an epitaxial $PbZr_{0.2}Ti_{0.8}O_3$ film we have established that ferroelectric nanodomains, created at the instance of localized polarization switching, produce a metallic conduction pathway through an otherwise insulating film. We hypothesize that metallic conductivity is mediated by tilted and curved domain-walls of the nanodomain, which cause localized carrier accumulation by virtue of their unique electrostatic and flexoelectric properties. Both theory and experiment have revealed that the carrier density and the metallic conductivity can be tuned by many orders of magnitude using only the average tilt of the domain wall with respect to the crystallographic axis. As a result, we have demonstrated the feasibility of recording multiple nonvolatile conductance states in a single metal-ferroelectirc contact, by varying only the size of the conducting nanodomains. These findings highlight the richness of polarization-coupled transport phenomena even in conventional ferroelectric materials. We anticipate that their extension onto thin films and atomically precise oxide superlattices of mutliferroics, mixed-phase, and antiferroelectrics will reveal a whole family of previously unknown electronic properties, paving way to new fundamental and applied prospects of oxide nanoelectronics.

■ ASSOCIATED CONTENT

Ⓢ Supporting Information

Experimental methods, supporting data on the conductivity of thicker films and domain walls in PZT, and a detailed theoretical analysis of local conductivity in ferroelectric semiconductors with tilted domain walls. This material is available free of charge via the Internet at http://pubs.acs.org.

■ AUTHOR INFORMATION

Corresponding Author

*E-mail: maksymovychp@ornl.gov.

■ ACKNOWLEDGMENTS

Experiments were carried out at the Center for Nanophase Materials Sciences, sponsored by the Division of User Facilities, Office of Basic Energy Sciences, U.S. Department of Energy. S.V.K. was supported by the U.S. Department of Energy, Basic Energy Sciences, Materials Sciences and Engineering Division. Material synthesis at Berkeley was partially supported by the SRC-NRI-WINS program as well as by the Director, Office of Science, Office of Basic Energy Sciences, Materials Sciences Division of the U.S. Department of Energy under contract No. DE-AC02-05CH1123.

■ REFERENCES

(1) Mannhart, J.; Schlom, D. G. *Science* **2010**, *327*, 1607−11.
(2) Ohtomo, A.; Hwang, H. Y. *Nature* **2004**, *427*, 423−6.
(3) Brinkman, A.; Huijben, M.; Zalk, M.; van; Huijben, J.; Zeitler, U.; Maan, J. C.; Wiel, W. G.; van der; Rijnders, G.; Blank, D. H. A.; Hilgenkamp, H. *Nat. Mater.* **2007**, *6*, 493−6.
(4) Okamoto, S.; Millis, A. J. *Nature* **2004**, *428*, 630−3.
(5) Santander-Syro, A. F.; Copie, O.; Kondo, T.; Fortuna, F.; Pailhès, S.; Weht, R.; Qiu, X. G.; Bertran, F.; Nicolaou, A.; Taleb-Ibrahimi, A.; Fèvre, P.; Le; Herranz, G.; Bibes, M.; Reyren, N.; Apertet, Y.; Lecoeur, P.; Barthélémy, A.; Rozenberg, M. J. *Nature* **2011**, *469*, 189−193.
(6) Meevasana, W.; King, P. D. C.; He, R. H.; Mo, S.-K.; Hashimoto, M.; Tamai, A.; Songsiriritthigul, P.; Baumberger, F.; Shen, Z.-X. *Nat. Mater.* **2011**, *10*, 114−118.
(7) Ueno, K.; Nakamura, S.; Shimotani, H.; Ohtomo, A.; Kimura, N.; Nojima, T.; Aoki, H.; Iwasa, Y.; Kawasaki, M. *Nat. Mater.* **2008**, *7*, 855−8.
(8) Borisevich, A.; Chang, H.; Huijben, M.; Oxley, M.; Okamoto, S.; Niranjan, M.; Burton, J.; Tsymbal, E.; Chu, Y.; Yu, P.; Ramesh, R.; Kalinin, S.; Pennycook, S. *Phys. Rev. Lett.* **2010**, *105*, 087204.
(9) Rondinelli, J.; Spaldin, N. *Phys. Rev. B* **2010**, *82*, 113402.
(10) Salje, E.; Zhang, H. *Phase Transitions* **2009**, *82*, 452−469.
(11) Chu, Y.-H.; He, Q.; Yang, C.-H.; Yu, P.; Martin, L. W.; Shafer, P.; Ramesh, R. *Nano Lett.* **2009**, *9*, 1726−30.
(12) Nelson, C. T.; Winchester, B.; Zhang, Y.; Kim, S.-J.; Melville, A.; Adamo, C.; Folkman, C. M.; Baek, S.-H.; Eom, C.-B.; Schlom, D. G.; Chen, L.-Q.; Pan, X. *Nano Lett.* **2011**, *11*, 828−34.
(13) Balke, N.; Choudhury, S.; Jesse, S.; Huijben, M.; Chu, Y. H.; Baddorf, A. P.; Chen, L. Q.; Ramesh, R.; Kalinin, S. V. *Nat. Nanotechnol.* **2009**, *4*, 868−75.
(14) Naumov, I. I.; Bellaiche, L.; Fu, H. X. *Nature* **2004**, *432*, 737−740.
(15) Vul, B. M.; Guro, G. M.; Ivanchik, I. I. *Ferroelectrics* **1973**, *6*, 29.
(16) Eliseev, E. A.; Morozovska, A. N.; Svechnikov, G. S.; Gopalan, V.; Shur, V. Y. *Phys. Rev. B* **2011**, *83*, 235313.
(17) Gureev, M.; Tagantsev, A.; Setter, N. *Phys. Rev. B* **2011**, *83*, 184104.
(18) Seidel, J.; Martin, L. W.; He, Q.; Zhan, Q.; Chu, Y.-H.; Rother, A.; Hawkridge, M. E.; Maksymovych, P.; Yu, P.; Gajek, M.; Balke, N.; Kalinin, S. V.; Gemming, S.; Wang, F.; Catalan, G.; Scott, J. F.; Spaldin, N. A.; Orenstein, J.; Ramesh, R. *Nat. Mater.* **2009**, *8*, 229−234.
(19) Guyonnet, J.; Gaponenko, I.; Gariglio, S.; Paruch, P. *Adv. Mater.* **2011**, DOI: 10.1002/adma.201102254.
(20) Seidel, J.; Maksymovych, P.; Batra, Y.; Katan, A.; Yang, S.-Y.; He, Q.; Baddorf, A.; Kalinin, S.; Yang, C.-H.; Yang, J.-C.; Chu, Y.-H.; Salje, E.; Wormeester, H.; Salmeron, M.; Ramesh, R. *Phys. Rev. Lett.* **2010**, *105*, 197603.
(21) Simmons, J. *Phys. Rev.* **1968**, *166*, 912−920.
(22) Maksymovych, P.; Pan, M.; Yu, P.; Ramesh, R.; Baddorf, A. P.; Kalinin, S. V. *Nanotechnology* **2011**, *22*, 254031.
(23) Garcia, V.; Fusil, S.; Bouzehouane, K.; Enouz-Vedrenne, S.; Mathur, N. D.; Barthélémy, A.; Bibes, M. *Nature* **2009**, *460*, 81−4.
(24) Gruverman, A.; Wu, D.; Lu, H.; Wang, Y.; Jang, H. W.; Folkman, C. M.; Zhuravlev, M. Y.; Felker, D.; Rzchowski, M.; Eom, C.-B.; Tsymbal, E. Y. *Nano Lett.* **2009**, *9*, 3539−43.
(25) Ahn, C. H.; Ventra, M.; Di; Eckstein, J. N.; Frisbie, C. D.; Gershenson, M. E.; Goldman, A. M.; Inoue, I. H.; Mannhart, J.; Millis, A. J.; Morpurgo, A. F.; Natelson, D.; Triscone, J.-M. *Rev. Mod. Phys.* **2006**, *78*, 1185−1212.
(26) Maksymovych, P.; Jesse, S.; Yu, P.; Ramesh, R.; Baddorf, A. P.; Kalinin, S. V. *Science* **2009**, *324*, 1421−1425.
(27) Stolichnov, I.; Tagantsev, A.; Setter, N.; Cross, J. S.; Tsukada, M. *Appl. Phys. Lett.* **1999**, *75*, 1790.
(28) Pintilie, L.; Vrejoiu, I.; Hesse, D.; LeRhun, G.; Alexe, M. *Phys. Rev. B* **2007**, *75*, 104103.
(29) Szot, K.; Dittmann, R.; Speier, W.; Waser, R. *Phys. Status Solidi* **2007**, *1*, R86−R88.
(30) Szot, K.; Speier, W.; Bihlmayer, G.; Waser, R. *Nat. Mater.* **2006**, *5*, 312−20.
(31) Spinelli, A.; Torija, M. A.; Liu, C.; Jan, C.; Leighton, C. *Phys. Rev. B* **2010**, *81*, 155110.
(32) Kalinin, S. V.; Rodriguez, B. J.; Jesse, S.; Maksymovych, P.; Seal, K.; Nikiforov, M.; Baddorf, A. P.; Kholkin, A. L.; Proksch, R. *Mat. Today* **2008**, *11*, 16−27.
(33) Morozovska, A. N.; Eliseev, E. A.; Li, Y.; Svechnikov, S. V.; Maksymovych, P.; Shur, V. Y.; Gopalan, V.; Chen, L.-Q.; Kalinin, S. V. *Phys. Rev. B* **2009**, *80*, 214110.
(34) Xiao, Y.; Shenoy, V.; Bhattacharya, K. *Phys. Rev. Lett.* **2005**, *95*, 247603.
(35) Tsymbal, E. Y.; Kohlstedt, H. *Science* **2006**, *313*, 181−3.